

Dynamics and fragmentation mechanism of $(\text{CH}_3\text{-C}_5\text{H}_4)\text{Pt}(\text{CH}_3)_3$ on SiO_2 Surfaces

Kaliappan Muthukumar¹, Harald O. Jeschke² and Roser Valentí^{*1}

Address: ¹Institut für Theoretische Physik, Goethe-Universität, Max-von-Laue-Straße 1, 60438 Frankfurt am Main, Germany and ²Research Institute for Interdisciplinary Science, Okayama University, 3-1-1 Tsushima-naka, Kita-ku, Okayama 700-8530, Japan

Email: Roser Valentí - valenti@itp.uni-frankfurt.de

* Corresponding author

Abstract

The interaction of $(\text{CH}_3\text{-C}_5\text{H}_4)\text{Pt}(\text{CH}_3)_3$ ((methylcyclopentadienyl)trimethylplatinum)) molecules on fully and partially hydroxylated SiO_2 surfaces, as well as the dynamics of this interaction were investigated using density functional theory (DFT) and finite temperature DFT-based molecular dynamics simulations. Fully and partially hydroxylated surfaces represent substrates before and after electron beam treatment and this study examines the role of electron beam pretreatment on the substrates in the initial stages of precursor dissociation and formation of Pt deposits. Our simulations show that on fully hydroxylated surfaces or untreated surfaces, the precursor molecules remain inactivated while we observe fragmentation of $(\text{CH}_3\text{-C}_5\text{H}_4)\text{Pt}(\text{CH}_3)_3$ on partially hydroxylated surfaces. The behavior of precursor molecules on the partially hydroxylated surfaces has been found to depend on the initial orientation of the molecule and the distribution of surface active sites. Based on the observations from the simulations and available experiments, we discuss possible dissociation channels of the precursor.

Keywords

$(\text{CH}_3\text{-C}_5\text{H}_4)\text{Pt}(\text{CH}_3)_3$; FEBID; EBID; Deposition; Precursor; Dissociation

Introduction

Nanoscale device applications require a growth of regular or specially patterned transition metal nanodeposits. Electron beam induced deposition (EBID), is a size and shape selective deposition process capable of writing low dimensional, sub-10 nm patterns on conducting and insulating substrates with tunable electronic properties [1-5]. However, the deposits obtained often contain less than 50 atomic % of metal which is detrimental to their conductivity. The incomplete dissociation of the precursor molecules on the substrate during the deposition process leaves a significant organic residue, thus impairing the quality of the deposits [4,6]. This lowers the range of applicability of EBID for nanotechnological applications. Several postfabrication approaches (such as annealing, post-deposition annealing in O₂, exposure to atomic hydrogen, post deposition electron irradiation) were proposed as viable techniques [7,8], but these approaches are not completely free from reproducibility issues. Therefore, to improve the metal content and to address the nature of the organic contamination, a fundamental understanding of how the molecules behave on the substrates is necessary. This will be helpful, either to modify the existing class of precursor materials or to design a novel set of precursors, specific for electron beam deposition. To address this, we have made a series of DFT studies in which we considered fully and partially hydroxylated SiO₂ surfaces as a representative for untreated and electron beam pretreated substrates and investigated the adsorption [9,10] and dynamics of several carbonyl precursors [11].

(CH₃-C₅H₄)Pt(CH₃)₃, in which Pt bonds directly to three methyl groups and a methylated cyclopentadienyl ring is a widely used precursor to obtain Pt deposits. Although the dissociation mechanism of (CH₃-C₅H₄)Pt(CH₃)₃, leading to the Pt deposit remains unknown, studies for a family of precursors similar to (CH₃-C₅H₄)Pt(CH₃)₃ in atomic layer deposition (ALD) conditions are available [12]. The studies in this review fairly agree that 1) the presence of surface hydroxyl groups are the source for the protons that help in the evolution of H₂, CH₄ and H₂O during the deposition process and 2) the molecules dissociate or associate through a ligand exchange process [13]. Recently, examination of the behavior of this molecule on fully hydroxylated SiO₂ surfaces has shown that the molecule remains physisorbed [14]. These static $T = 0$ K DFT computations provide

insights on the bonding of $(\text{CH}_3\text{-C}_5\text{H}_4)\text{Pt}(\text{CH}_3)_3$ to this surface, but are limited to the adsorption behavior of the molecule. Several questions remain, such as the behavior of $(\text{CH}_3\text{-C}_5\text{H}_4)\text{Pt}(\text{CH}_3)_3$ on electron beam pretreated substrates, the role of temperature in the dissociation of the precursor on untreated surfaces, and the possible mechanism by which the precursor dissociates on the electron beam pretreated surfaces.

Hence, in order to extend the knowledge on the adsorption and to address the open questions in the deposition process, in this study we use DFT and finite temperature DFT-based molecular dynamic simulations (MD) and investigate the adsorption behavior of $(\text{CH}_3\text{-C}_5\text{H}_4)\text{Pt}(\text{CH}_3)_3$ on fully and partially hydroxylated SiO_2 surfaces. We focus on explaining the initial reactions and the possible fragmentation pathways of the $(\text{CH}_3\text{-C}_5\text{H}_4)\text{Pt}(\text{CH}_3)_3$ molecule on the SiO_2 surface and we explain the nature of organic contamination in the deposits.

Computational Details

DFT calculations for the substrates, $(\text{CH}_3\text{-C}_5\text{H}_4)\text{Pt}(\text{CH}_3)_3$ precursor molecules, and the combined substrate/precursor molecule system were performed using the projector augmented wave (PAW) method [15,16] as implemented in the Vienna Ab-initio Simulation Package (VASP-5.2.11) [17-19]. The generalized gradient approximation in the parameterization of Perdew, Burke and Ernzerhof [20] was used as approximation for the exchange and correlation functional. In addition, dispersion corrections [21] were used to simulate the long range van der Waals interactions. All calculations were performed in the scalar relativistic approximation. A kinetic energy cut-off of 400 eV was used and all ions were fully relaxed using a conjugate gradient scheme until the forces were less than 0.01 eV/Å. In the geometry optimizations for the molecule and the surface models the Brillouin zone was sampled at the Γ point only. Spin polarization was considered for all calculations. Different spin states (i.e. in each case the two lowest possible spin states) were considered, and only the results of the ground state are reported below. The adsorption energy (E_A) was defined as $E_A \equiv \Delta E = E_{\text{total}} - E_{\text{substrate}} - E_{\text{adsorbate}}$, where E_{total} , $E_{\text{substrate}}$, and $E_{\text{adsorbate}}$ are the energies of the combined

system (adsorbate and the slab), of the slab, and of the adsorbate molecule in the gas phase in a neutral state, respectively.

The most stable systems were considered for studying the dynamics of the adsorbed precursor molecule. MD simulations were performed for 20 ps on a canonical ensemble at a finite temperature of $T = 600\text{ K}$ using the Nose-Hoover thermostat [22]. The temperature 600 K [23] was chosen in accordance with a typical experiment used for $(\text{CH}_3\text{-C}_5\text{H}_4)\text{Pt}(\text{CH}_3)_3$ deposition. The Verlet algorithm in its velocity form with a time step of $\Delta t = 1\text{ fs}$ was used to integrate the equations of motion. For these simulations, we have used a reduced $(2\times 2\times 2)$ SiO_2 supercell so as to reduce the computational time. For reaction modeling studies, all species (transition states (TS) and intermediates (INT)) in the proposed reaction paths in Fig. 5 were traced at PM6 (Parametrized Model 6) level using the Berny algorithm implemented in Gaussian-09 software [24].

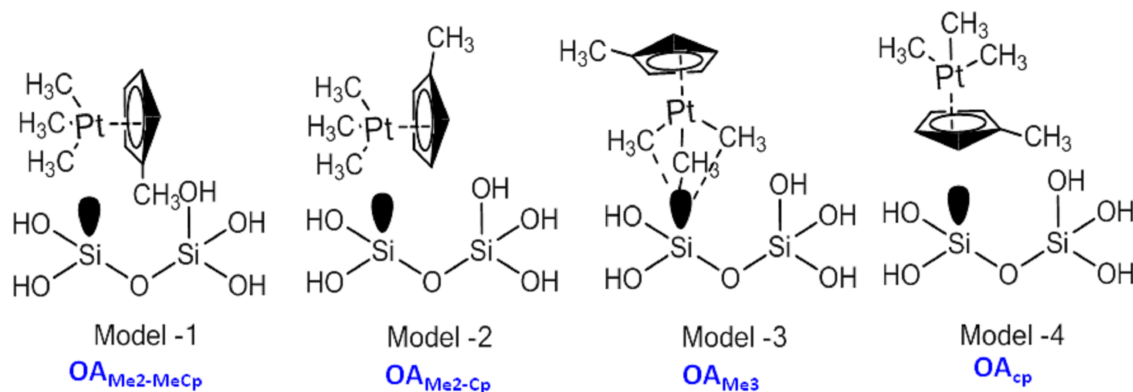
Results and Discussion

Adsorption of $(\text{CH}_3\text{-C}_5\text{H}_4)\text{Pt}(\text{CH}_3)_3$ on SiO_2 substrates

The interaction of the precursor molecule with the substrate, in general, depends on both the orientation of the adsorbate and the adsorption site on the substrate. The interaction of $(\text{CH}_3\text{-C}_5\text{H}_4)\text{Pt}(\text{CH}_3)_3$ with the fully hydroxylated SiO_2 substrate surfaces was investigated by placing the molecule with different orientations on several bonding sites and the most stable configuration is the one in which the methylcyclopentadienyl ring and two of the methyl groups that are directly bonded to Pt are oriented towards the substrate [14].

In a similar way, the bonding of $(\text{CH}_3\text{-C}_5\text{H}_4)\text{Pt}(\text{CH}_3)_3$ precursor molecules on partially hydroxylated SiO_2 surfaces were investigated. The initial configurations of $(\text{CH}_3\text{-C}_5\text{H}_4)\text{Pt}(\text{CH}_3)_3$ considered for simulations on the partially hydroxylated surfaces are shown schematically in Figure 1. We simulate the precursor adsorption on two different partially hydroxylated surface models, that differ in the number of available active sites on the surfaces; 11% (Figure 1 upper panel) and 22% (Figure 1 lower panel). On these surfaces, two sets of $(\text{CH}_3\text{-C}_5\text{H}_4)\text{Pt}(\text{CH}_3)_3$ orientations were considered; (1) reclining orientations (Model-1/1a and Model-2/2a)), that differ in the orientation of

Case -1 - POH surfaces with 11% defects



Case -2 - POH surfaces with 22% defects

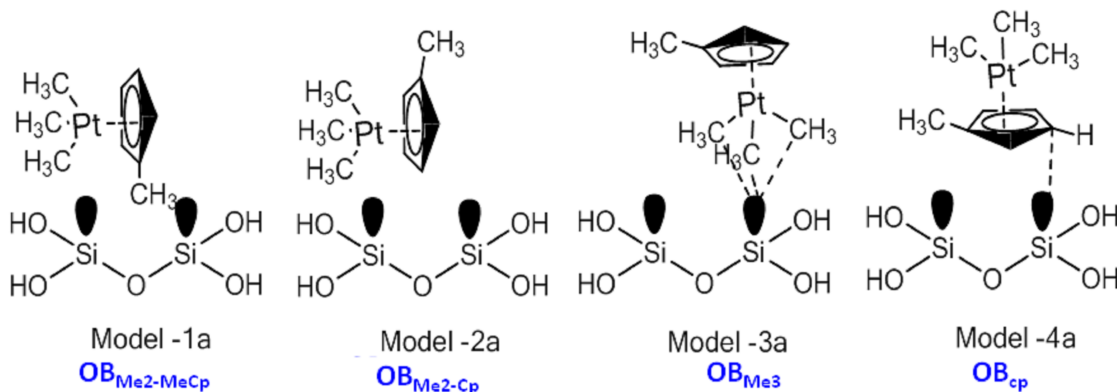


Figure 1: Schematic representation of the initial orientations of $(CH_3-C_5H_4)Pt(CH_3)_3$ on 11% (Model-1 to 4, upper panel) and 22% (Model-1a to 4a, lower panel) partially dehydroxylated surfaces.

the methylcyclopentadienyl ring of $(CH_3-C_5H_4)Pt(CH_3)_3$, and (2) upright configurations (Model-3/3a) and Model-4/4a)) in which either three of the CH_3 groups bonded to Pt or the centroid of the methylcyclopentadienyl ring bonds to the substrate. These initial configurations are allowed to relax without any constraints. The configurations where $(CH_3-C_5H_4)Pt(CH_3)_3$ is placed on the bridging sites move spontaneously to on-top sites during geometry relaxation and hence are not discussed further. The calculated adsorption energies (E_A) are summarized in Table and the configurations in Fig. 2.

The calculated values of (E_A) of $(CH_3-C_5H_4)Pt(CH_3)_3$ on 11% partially dehydroxylated surfaces indicates that the most stable configurations are Model-2 (OA_{Me2Cp} $E_A = -1.443$ eV) and Model-4 (OA_{Cp} , $E_A = -1.458$ eV) given in Figure 2 (a) and (b)). The configurations are equally stable

Table 1: Adsorption energies of $(\text{CH}_3\text{-C}_5\text{H}_4)\text{Pt}(\text{CH}_3)_3$ on partially hydroxylated SiO_2 surfaces with 11 and 22% defects. The cases listed correspond to configurations in Fig. 1. All values in eV/unit cell.

Cases	SiO ₂ surfaces with	
	11% defects	22% defects
Model-1/1a	-0.680	-2.321
Model-2/2a	-1.443	-2.297
Model-3/3a	-0.332	-2.769
Model-4/4a	-1.458	-2.360

within computational error. The configurations Model-1 ($\text{OA}_{\text{Me}_2\text{MeCp}}$, $E_A = -0.680$ eV) and Model-3 (OA_{Me_3} , $E_A = -0.332$ eV) are less stable and are not considered for discussion. In Model-4, where the centroid of the methylcyclopentadienyl ring is oriented on top of a Si atom in the initial configuration, a spontaneous bond formation between one of the carbon atoms of the ring and the surface Si atom is observed during relaxation. There has been no evidence of any further dissociation.

Bonding of $(\text{CH}_3\text{-C}_5\text{H}_4)\text{Pt}(\text{CH}_3)_3$ has also been considered on the 22% partially dehydroxylated surfaces and the relaxed configurations are shown in Fig. 2 (c-e). The calculated adsorption energies for the reclining configurations Model-1a ($\text{OB}_{\text{Me}_2\text{MeCp}}$, and Model-2a ($\text{OB}_{\text{Me}_2\text{Cp}}$) are -2.321 and -2.297 eV, respectively. We do not observe any spontaneous dissociation on these configurations. However, when the relaxations are started with Model-3a orientation (OB_{Me_3}) a stronger adsorption with an $E_A = -2.769$ eV is observed. In this case, one of the three CH_3 groups that bonds directly to the Pt atom dissociates, as has been observed on the experimental investigations [4,25-28]. The detached CH_3 group was found to bind to one of the surface active sites. However, this situation was not observed on 11% partially dehydroxylated surfaces indicating that the dissociation is assisted by the neighboring active site, which is present on the 22% partially dehydroxylated surfaces. The next most stable configurations on the 22% partially dehydroxylated surface are obtained from Model-4a ((OB_{Cp}) $E_A = -2.360$ eV).

A comparison of the calculated adsorption energies for the 11% and 22% cases indicates that the molecules are more stable on the latter. Furthermore, no dissociation on the 11% dehydroxylated surfaces was observed. These observations illustrate that the orientation of $(\text{CH}_3\text{-C}_5\text{H}_4)\text{Pt}(\text{CH}_3)_3$ on

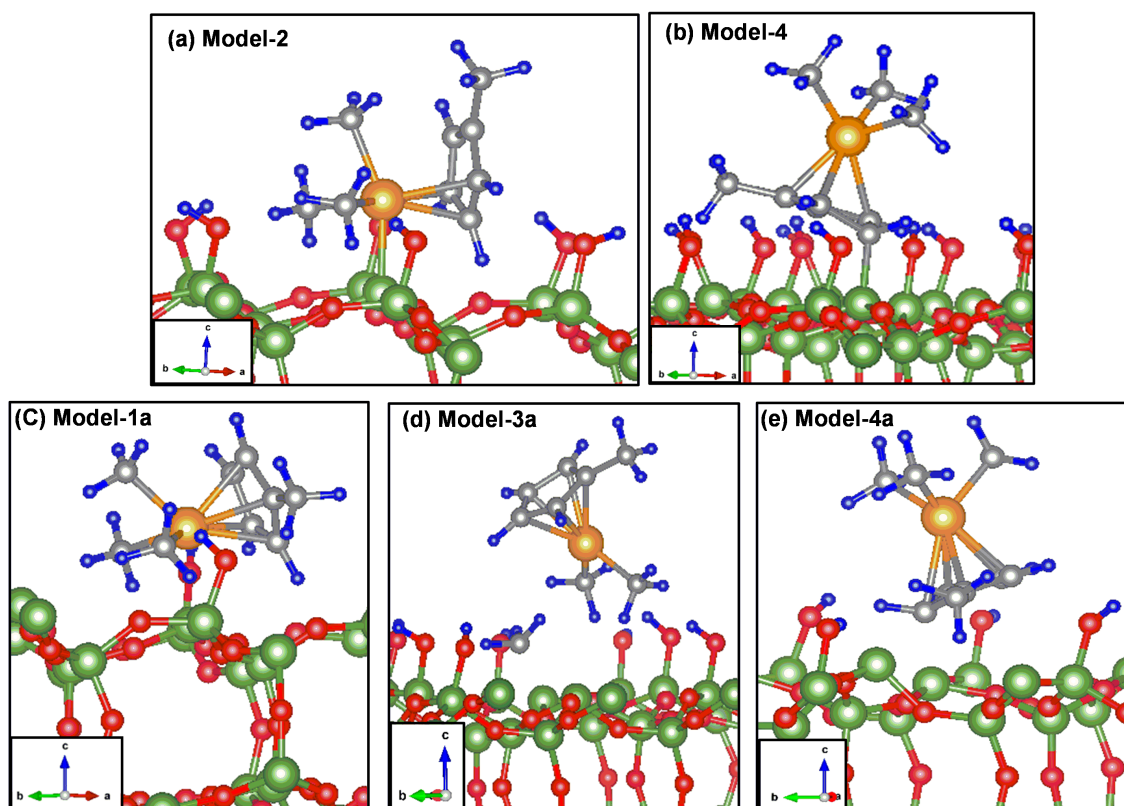


Figure 2: Relaxed structures of $(\text{CH}_3\text{-C}_5\text{H}_4)\text{Pt}(\text{CH}_3)_3$ on the 11% ((a), (b)) and 22% ((c)-(e)) partially dehydroxylated surfaces. The labels correspond to the initial configurations shown in Fig. 1. In the most stable configuration for the 22% case (panel d) one of the three methyl groups bonded to Pt dissociates spontaneously during relaxation. Color code: green - Si, red - O, orange - Pt, gray - C and blue - H throughout this manuscript. To better display the changes occurring the system in 2D view, the snapshots have slightly different orientations in the ab plane (note the coordinate systems).

SiO_2 surfaces, and the availability and location of active sites on the surface are crucial factors in dictating the dissociation of precursors and the growth mechanism of deposits.

Dynamics of the $(\text{CH}_3\text{-C}_5\text{H}_4)\text{Pt}(\text{CH}_3)_3$ Precursor on SiO_2 substrates

To gain further insight on the growth process of Pt deposits, dynamics of $(\text{CH}_3\text{-C}_5\text{H}_4)\text{Pt}(\text{CH}_3)_3$ on both fully and partially hydroxylated surfaces were simulated. Due to the high computational expense however, a reduced $2 \times 2 \times 2$ supercell of SiO_2 (see Figure 3 (a)), was used. This reduced supercell provides a closer packing of precursor molecules (the nearest neighbor distance between two Pt atoms in $(\text{CH}_3\text{-C}_5\text{H}_4)\text{Pt}(\text{CH}_3)_3$ is ca. 8 Å in the reduced cell compared to ca. 15 Å in the

original supercell) and an enhanced concentration of surface hydroxyl vacancies is provided in the reduced cell on partially dehydroxylated surfaces (i.e, 25% and 50% compared to 11% and 22%). However, the environment around these sites is similar (i.e., the sites are isolated on the 25% partially dehydroxylated surface and located adjacent to each other on the 50% partially dehydroxylated surface).

Table 2: Comparison of $(\text{CH}_3\text{-C}_5\text{H}_4)\text{Pt}(\text{CH}_3)_3$ adsorption energies on the $3 \times 3 \times 4$ supercell and the reduced $2 \times 2 \times 2$ supercell. For the fully hydroxylated surfaces, the values are taken from ref. [14]. Model-2 and 4 are the stable configurations of $(\text{CH}_3\text{-C}_5\text{H}_4)\text{Pt}(\text{CH}_3)_3$ on partially hydroxylated surfaces. All values in eV.

Cases	Supercells	
	$3 \times 3 \times 4$	$2 \times 2 \times 2$
Fully hydroxylated – $(\text{OMe}_2\text{MeCp})$	-0.650	-1.02
Fully hydroxylated – (OMe_2Cp)	-0.596	-0.845
Model – 2	-1.443	-1.494
Model – 4	-1.458	-1.647

Selected configurations on fully and partially hydroxylated SiO_2 surfaces are computed on this reduced supercell and compared for consistency (Table 2). We observe a similar trend for the energetics and the order of stabilization of configurations as in the $3 \times 3 \times 4$ cell. For example, the most stable configuration for $(\text{CH}_3\text{-C}_5\text{H}_4)\text{Pt}(\text{CH}_3)_3$ on the fully hydroxylated surfaces (Figure 3 (b)) of both of these cells are similar. The $(\text{CH}_3\text{-C}_5\text{H}_4)\text{Pt}(\text{CH}_3)_3$ adsorption on $3 \times 3 \times 4$ fully hydroxylated surface slabs has the most stable configuration as $\text{OMe}_2\text{-MeCp}$ ($E_A = -0.650$ eV) followed by $\text{OMe}_2\text{-Cp}$ ($E_A = -0.596$ eV) [14]. On a $2 \times 2 \times 2$ supercell, the most stable configuration is $\text{OMe}_2\text{-MeCp}$ ($E_A = -1.02$ eV) followed by $\text{OMe}_2\text{-Cp}$ ($E_A = -0.845$ eV). Analogously, on a $3 \times 3 \times 4$ partially hydroxylated surface, the most stable configuration is Model-4 ($E_A = -1.458$ eV) followed by Model-2 ($E_A = -1.443$ eV) and a similar trend is observed with the reduced supercell i.e., Model-4 ($E_A = -1.647$ eV) followed by Model-2 ($E_A = -1.494$ eV). Nevertheless, the calculated E_A on the reduced supercell is higher than those when using the $3 \times 3 \times 4$ slabs, owing to the enhanced concentration of the hydroxyl groups and defective sites and closer packing of the molecules. On the 50% dehydroxylated cells, where two surface active sites are located adjacent to each other, one of the CH_3 groups which was originally bonded to Pt, fragments and bonds to the adjacent vacant

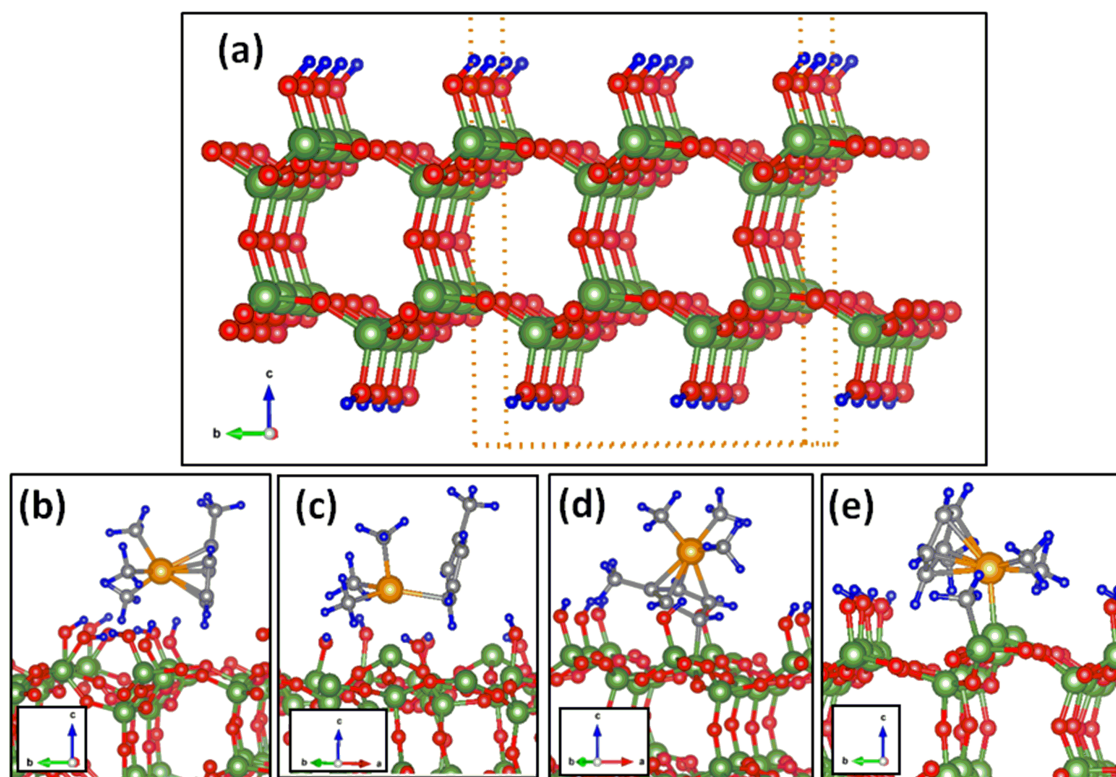


Figure 3: (a) Reduced supercell with the fully hydroxylated SiO₂ considered for the molecular dynamics simulations. (b-e) Most stable configurations of (CH₃-C₅H₄)Pt(CH₃)₃ (b) on the fully hydroxylated surface, (c) and (d) 25% and (e) 50% partially dehydroxylated surfaces.

site, as observed in the $3 \times 3 \times 4$ cell (See Fig. 2 (d) and Fig. 3 (e)). These DFT relaxed structures (as shown in Fig. 3 (b-e) are considered as starting point for molecular dynamics simulations.

The trajectory of the MD simulations for the four considered cases are shown in Fig. 4. The analysis of the trajectory indicates that on the fully hydroxylated surfaces (Fig. 4 (a)) the molecule exhibits significant changes in orientation and a drift similar as we found for carbonyl precursors [11]. The Pt-Cp ring and Pt-CH₃ fluctuate to a maximum of 5% and 1%, respectively. Apart from this, in the simulation window, we do not observe any further indications on the dissociation of the precursor molecules. The trajectory of MD simulations and arising configurations of (CH₃-C₅H₄)Pt(CH₃)₃ on the (25% and 50%) partially dehydroxylated SiO₂ surfaces in MD simulations are shown in Figs. 4 (b)-(d). When simulation is started with the configuration shown in Figure 3 (b), a significant bond weakening (Pt-Cp ring and Pt-CH₃) is observed (Fig. 4 (b)). Quantitatively, the respective bond fluctuations computed for Pt-Cp ring and Pt-CH₃ bonds were 11% and 9%, respectively. However,

when MD simulations are performed with Fig. 3 (d) as starting configuration, where a part of the methylcyclopentadienyl ring is bonded to the surface Si atom during the simulations, the bonding of that part with the $\text{Pt}(\text{CH}_3)_3$ part of the precursor is weakened. When simulations are extended further, the $\text{Pt}(\text{CH}_3)_3$ part detaches and moves to the vacuum leaving the methylcyclopentadienyl ring bonded to the substrate (see Fig. 4 (c)). On the 50% partially dehydroxylated surface, (Fig. 4 (d)), no further association or dissociation of methyl groups or detachment of methylcyclopentadienyl rings are observed.

These results illustrate that the $(\text{CH}_3\text{-C}_5\text{H}_4)\text{Pt}(\text{CH}_3)_3$ precursor molecules exhibit a tendency to fragment upon their interaction with the partially hydroxylated sites and a drifting without fragmentation of molecules on the fully hydroxylated surfaces. On the partially hydroxylated surfaces, the dissociation begins either with the release of one of the methyl groups bonded directly to Pt or the detachment of the methylcyclopentadienyl ring. This indicates that surface active sites are necessary for the fragmentation of precursor molecules and this is because of the electron density located on the Si atoms, which is crucial for bonding with the precursor molecule and further fragmentation [9,10]. The 25 and 50% partially dehydroxylated surfaces represent electron beam pretreated surfaces and therefore the pretreatment of the substrate with the electron beam helps in favoring dissociation of the precursor molecule and efficient deposition. Since during the MD simulations we do not observe the dissociation of methylcyclopentadienyl ring or the release of CH_3 from the surface Si sites, it is expected that they might block the active sites from the approach of incoming precursor molecules.

Pathways for $(\text{CH}_3\text{-C}_5\text{H}_4)\text{Pt}(\text{CH}_3)_3$ precursor fragmentation

In order to further understand the nature of interaction of $(\text{CH}_3\text{-C}_5\text{H}_4)\text{Pt}(\text{CH}_3)_3$ with partially hydroxylated SiO_2 surfaces, the barriers for adsorption and fragmentation of these molecules to the partially hydroxylated groups were simulated. For this purpose, a representative simple cluster model $\text{Si}(\text{OH})_3$ is considered. Although this does not account for the complete surface model, it is a good approximation to evaluate the reaction barriers for different reactions observed through the MD simulations. In the literature, such a simple hydroxylated $\text{M}(\text{OH})_x$ model has been used as a

representative model to investigate deposition reactions on Al [29], Hf [13] and Si [30-32]. Also, the energies reported in this section are computed at the PM6 level of theory, and a relative comparison should enable reasonable understanding of the possible fragmentation pathways qualitatively. In a recent investigation, thickness controlled site-selective Pt deposits were obtained by the direct ALD (Atomic layer deposition) process, in which ALD was performed on EBID patterned substrates. In this ALD process, an O₂ pulse is used to obtain better nucleation, even though the qualitative understanding of the role of O₂ remains uncertain. Therefore, in this section we consider involvement of O₂ in the pathways at different stages of the reaction and calculate the energetics to compare and elucidate the role of O₂ [33].

Our simulations of the adsorption and dynamics of (CH₃-C₅H₄)Pt(CH₃)₃ on SiO₂ surfaces show that the dissociation begins with either the detachment of CH₃ groups or the methylcyclopentadienyl ring. In the cluster model, the interaction of (CH₃-C₅H₄)Pt(CH₃)₃ with the surface Si atoms, has a barrier of 0.140 eV, when (CH₃-C₅H₄)Pt(CH₃)₃ interacts through the methylcyclopentadienyl ring. Removal of the methylcyclopentadienyl ring from (CH₃-C₅H₄)Pt(CH₃)₃ has an activation energy of +0.771 eV, which leaves the Pt(CH₃)₃ part of the precursor binding to the substrate. Formation of Pt(CH₃)₃ on vacuum is observed in our molecular dynamics simulations. However, neither its dissociation into vacuum or adsorption back to the surface Si sites has not been observed. Therefore, for analyzing the dissociation channels of Pt(CH₃)₃, we reasonably approximate our starting configuration as Pt(CH₃)₃ bonded with the surface Si site as shown in Figure 5. Our adsorption studies reveal that for the elimination of methyl groups, two surface active sites are necessary, and the present model limits the computation of barrier for such cases.

Possible pathways by which Pt(CH₃)₃ gets dissociated on the model cluster, in the presence and absence of O₂, are derived and shown in Scheme 5. From Pt(CH₃)₃, the release of one CH₃ group (P1TS1) forming Pt(CH₃)₂ has an activation energy of about +1.073 eV compared to +1.617 eV for ethane release (P2TS1). The O₂ assisted elimination of first methyl (P3TS1) from Pt(CH₃)₃ has a barrier of +3.699 eV. Therefore, release of a first CH₃ is expected to proceed through P1TS1, leaving Pt(CH₃)₂ (P1-PRO-1) on the Si surface. The removal of the second and third CH₃ from Pt(CH₃)₂

can happen by a number of ways ((PATH A-D, see Fig. 5 and Fig. 6). Ethane elimination, which leads to a Pt atom (PA-TS1) bonded to the Si surface has a barrier of about +1.989 eV. This reaction is exothermic by -0.798 eV. The first step (PBTS-1) in Path-B, leading to second methyl elimination has a barrier of +0.724 eV, and occurs in a similar fashion as the first methyl removal. This reaction resulting in species (PBINT-1) is exothermic by -0.207 eV. Comparing the pathways considered and the computed activation energies as shown in Figure 6), the third methyl elimination in the presence of oxygen and the subsequent formation of Pt-oxy species (Path-B, C, D) have a high activation barrier.

The formed Pt or Pt-oxy species might agglomerate and form Pt deposits and the role of O_2 on this process hasn't been explored in this investigation. Some experimental studies were available and possible mechanisms were proposed [34]. Simulations in this study were performed at the PM6 level, with no corrections for weak interactions and at $T = 0$ K. Taking into account the temperature of most processes, which range between 200 and 400 °C, some of the high-barrier pathways might also be operative. Also, the role of secondary electrons and the point defects which might occur as a result of electron impingement on the surface have not been explored. This study therefore provides a preliminary understanding of how the $(CH_3-C_5H_4)Pt(CH_3)_3$ molecule can dissociate on the substrates that qualitatively represent electron beam pretreated surfaces.

CONCLUSIONS

We have performed theoretical simulations on the dynamics and fragmentation mechanisms of $(CH_3-C_5H_4)Pt(CH_3)_3$ on the fully and partially hydroxylated SiO_2 surfaces. Our results provide clues for the most stable configurations of $(CH_3-C_5H_4)Pt(CH_3)_3$ on SiO_2 surfaces and their dynamical behavior. These results illustrate that the fragmentation of the precursor molecule begins with either the detachment of either the methylcyclopentadienyl ring or the methyl group. Detached methylcyclopentadienyl rings and the dissociated CH_3 groups block the surface active sites and might be the source of organic contamination. Since the composition of the obtained deposits dictate the conductance behavior, it can be speculated that a design of suitable precursors for electron beam

induced deposition might be more efficient than the use of traditional ALD precursors. With our reaction modeling studies, possible pathways by which the precursor molecule can fragment on SiO₂ surfaces were also explored.

Acknowledgments

The authors gratefully acknowledge financial support by the Beilstein-Institut, Frankfurt/Main, Germany, and the EU COST action CELINA. The generous allotment of computer time by CSC-Frankfurt and LOEWE-CSC is gratefully acknowledged.

References

1. Wnuk, J. D.; Rosenberg, S. G.; Gorham, J. M.; van Dorp, W. F.; Hagen, C. W.; Fairbrother, D. *H. Surf. Sci.* **2011**, *605*, 257.
2. Utke, I.; Hoffmann, P.; Melngailis, J. *J. Vac. Sci. Technol. B* **2008**, *26*, 1197.
3. Weber, M.; Rudolph, M.; Kretz, J.; Koops, H. W. P. *J. Vac. Sci. Technol. B* **1995**, *13*, 461.
4. Wnuk, J. D.; Gorham, J. M.; Rosenberg, S. G.; van Dorp, W. F.; Madey, T. E.; Hagen, C. W.; Fairbrother, D. H. *J. Phys. Chem. C* **2009**, *113*, 2487.
5. Weirich, P. M.; Winhold, M.; Schwalb, C. H.; Huth, M. *Beilstein J. Nanotechnol.* **2013**, *4*, 919.
6. Hedhili, M. N.; Bredehft, J. H.; Swiderek, P. *J. Phys. Chem. C* **2009**, *113*, 13282.
7. Huth, M.; Porrati, F.; Schwalb, C.; Winhold, M.; Sachser, R.; Dukic, M.; Adams, J.; Fantner, G. *Beilstein J. Nanotechnol.* **2009**, *3*, 597.
8. Lewis, B. B.; Stanford, M. G.; Fowlkes, J. D.; Lester, K.; Plank, H.; Rack, P. D. *Beilstein J. Nanotechnol.* **2015**, *6*, 907.
9. Muthukumar, K.; Opahle, I.; Shen, J.; Jeschke, H. O.; Valentí, R. *Phys. Rev. B* **2011**, *84*, 205442.

10. Muthukumar, K.; Jeschke, H. O.; Valentí, R.; Begun, E.; Schwenk, J.; Porрати, F.; Huth, M. *Beilstein J. Nanotechnol.* **2012**, *3*, 546.
11. Muthukumar, K.; Jeschke, H. O.; Valentí, R. *J. Chem. Phys.* **2014**, *140*, 184706.
12. George, S. M. *Chem. Rev.* **2010**, *110*, 111.
13. Mastail, C.; Lanthony, C.; Olivier, S.; Ducéré, J.-M.; Landa, G.; Estève, A.; Rouhani, M. D.; Richard, N.; Dkhissi, A. *Thin Solid Films* **2012**, *520*, 4559.
14. Shen, J.; Muthukumar, K.; Jeschke, H. O.; Valentí, R. *New. J. Phys.* **2012**, *14*, 073040.
15. Blöchl, P. E. *Phys. Rev. B* **1994**, *50*, 17953.
16. Kresse, G.; Joubert, D. *Phys. Rev. B* **1999**, *59*, 1758.
17. Kresse, G.; Furthmüller, J. *Phys. Rev. B* **1996**, *54*, 11169.
18. Kresse, G.; Furthmüller, J. *Comput. Mater. Sci.* **1996**, *6*, 15.
19. Kresse, G.; Hafner, J. *Phys. Rev. B* **1993**, *47*, 558.
20. Perdew, J. P.; Burke, K.; Ernzerhof, M. *Phys. Rev. Lett.* **1996**, *77*, 3865.
21. Grimme, S. *J. Comput. Chem.* **2006**, *27*, 1787.
22. Hafner, J. *J. Comput. Chem.* **2008**, *29*, 2044.
23. Dendooven, J.; Ramachandran, R. K.; Casier, K. D.; Rampelberg, G.; Filez, M.; Poelman, H.; Marin, G. B.; Fonda, E.; Detavernier, C. *J. Phys. Chem. C* **2013**, *117*, 20557.
24. Gaussian 09, Revision A.02; Gaussian, Inc.: Wallingford, CT, 2016.
25. Egger, K. W. *J. Organometal. Chem.* **1970**, *24*, 501.
26. Spencer J. A.; Rosenberg, G. S.; Barclay, M.; Wu Y-C.; McElwee-White L.; Fairbrother H.D.; *Appl. Phys. A* **2014**, *117*, 1631.

27. Liang, X.; Zhou, Y.; Li, J.; Weimer, A. W. *J. Nanopart. Res.* **2011**, *13*, 3781.
28. Koplitz, L. V.; Shuh, D. K.; Chen, Y.-J.; Williams, R. S.; Zink, J. I. *Appl. Phys. Lett.* **1988**, *53*, 1705.
29. Widjaja, Y.; Musgrave, C. B. *Appl. Phys. Lett.* **1999**, *80*, 3304.
30. Mukhopadhyay, A. B.; Musgrave, C. B. *Chem. Phys. Lett.* **2006**, *421*, 215.
31. Hu, Z.; Turner, C. H. *J. Phys. Chem. B* **2006**, *110*, 8337.
32. Dkhissi, A.; Esteve, A.; Jeloica, L.; Djafari Rouhani, M.; Landa, G. *Chem. Phys.*, **2006**, *323*, 179.
33. Mackus, A. J. M.; Thissen, N. F. W.; Mulders, J. J. L.; Trompenaars, P. H. F.; Verheijen, M. A.; Bol, A. A.; Kessels, W. M. M. *J. Phys. Chem. C* **2013**, *117*, 10788.
34. Stanford, M. G.; Lewis, B. B.; Noh J. H.; Fowlkes, D. J.; Roberts, A. N.; Plank, H.; Rack, P.D; *ACS Appl. Mater. Interfaces* **2014**, *6*, 21256.

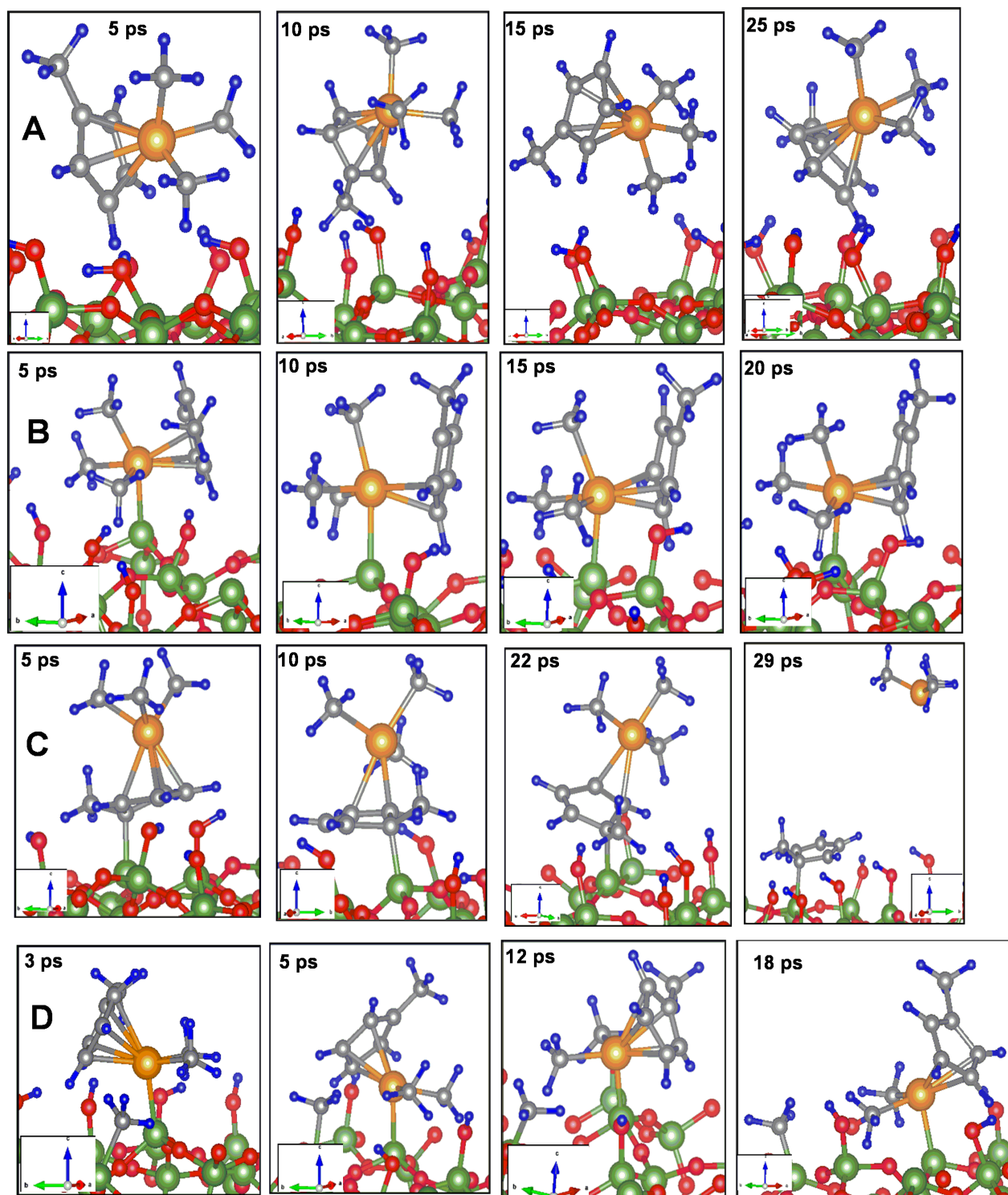


Figure 4: The configurations of $(\text{CH}_3\text{-C}_5\text{H}_4)\text{Pt}(\text{CH}_3)_3$ obtained from molecular dynamics simulations (20 ps) on (a) fully hydroxylated surfaces, (b)-(c) 25% and (d) 50% partially dehydroxylated surfaces

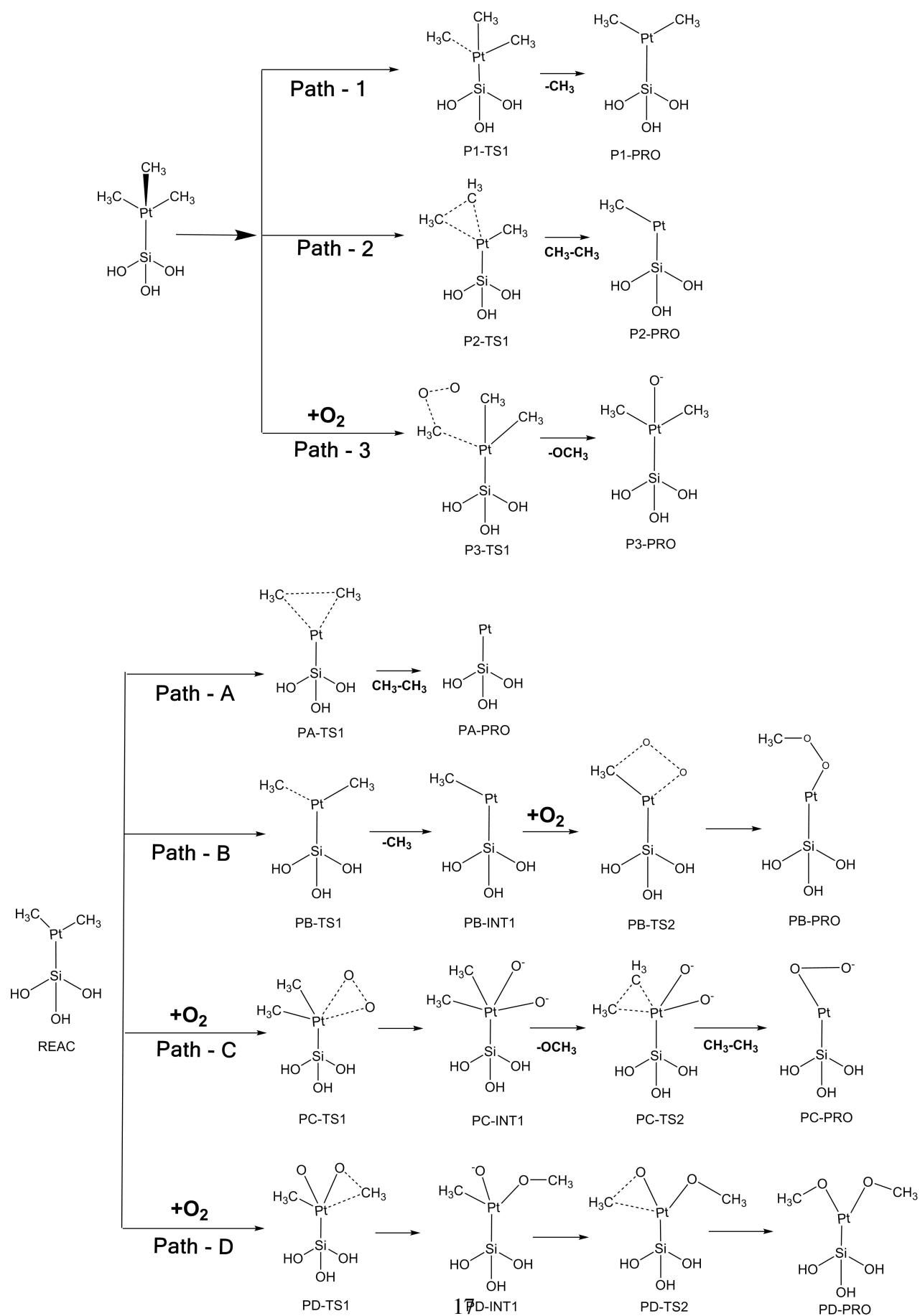


Figure 5: Possible reaction channels for the dissociation of $(\text{CH}_3\text{-C}_5\text{H}_4)\text{Pt}(\text{CH}_3)_3$ after its interaction with partially hydroxylated SiO_2 surfaces and in an O_2 environment. Possible pathways for

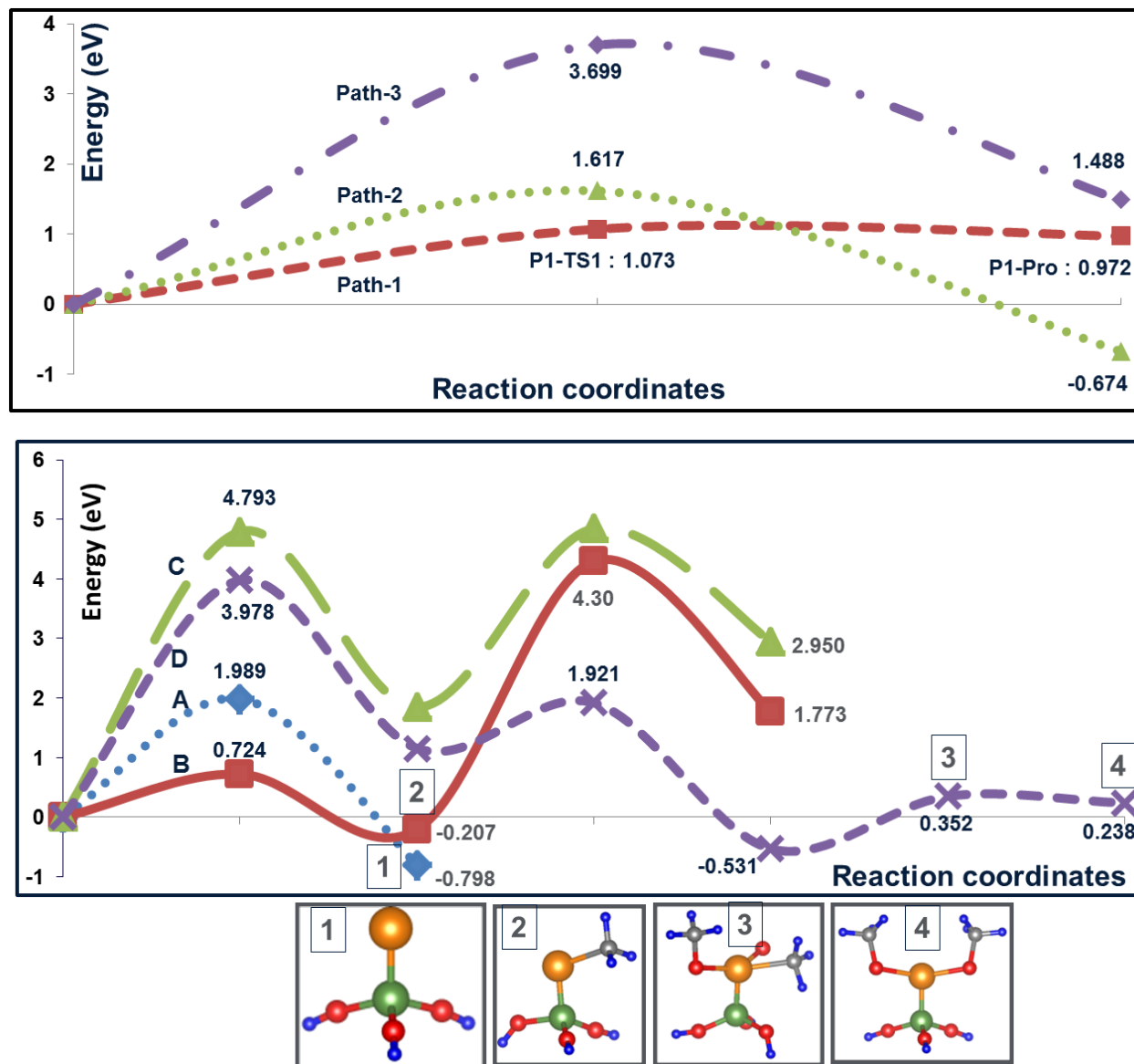


Figure 6: Energetics for different pathways (PATH 1-3 and A-D) considered for the dissociation of precursor molecules. Representative figures are displayed.